THE JOURNAL OF BIOLOGICAL CHEMISTRY VOL. 281, NO. 9, pp. 5992–5999, March 3, 2006

Proteoglycan Mechanics Studied by Single-molecule Force Spectroscopy of Allotypic Cell Adhesion Glycans*

Received for publication, July 20, 2005, and in revised form, December 13, 2005 Published, JBC Papers in Press, December 22, 2005, DOI 10.1074/jbc.M507878200

Sergi Garcia-Manyes[‡§1], Iwona Bucior[¶‖], Robert Ros[**], Dario Anselmetti[**], Fausto Sanz[§], Max M. Burger[¶‖], and Xavier Fernàndez-Busquets[‡‖2]

From the [‡]Research Center for Bioelectronics and Nanobioscience, Barcelona Science Park, University of Barcelona , Josep Samitier 1-5, Barcelona E-08028, Spain, the [§]Departament de Química Física, University of Barcelona, Martí i Franquès 1, Barcelona E-08028, Spain, the [¶]Friedrich Miescher-Institut, Basel CH-4002, Switzerland, the [‖]Marine Biological Laboratory, Woods Hole, Massachusetts 02543, and the [**]Department of Experimental Biophysics and Applied Nanoscience, University of Bielefeld, Physics Faculty, Universitätsstrasse 25, Bielefeld D-33615, Germany

Early Metazoans had to evolve the first cell adhesion system addressed to maintaining stable interactions between cells constituting different individuals. As the oldest extant multicellular animals, sponges are good candidates to have remnants of the molecules responsible for that crucial innovation. Sponge cells associate in a species-specific process through multivalent calcium-dependent interactions of carbohydrate structures on an extracellular membrane-bound proteoglycan termed aggregation factor. Single-molecule force spectroscopy studies of the mechanics of aggregation factor self-binding indicate the existence of intermolecular carbohydrate adhesion domains. A 200-kDa aggregation factor glycan (g200) involved in cell adhesion exhibits interindividual differences in size and epitope content which suggest the existence of allelic variants. We have purified two of these g200 distinct forms from two individuals of the same sponge species. Comparison of allotypic *versus* isotypic g200 binding forces reveals significant differences. Surface plasmon resonance measurements show that g200 self-adhesion is much stronger than its binding to other unrelated glycans such as chondroitin sulfate. This adhesive specificity through multiple carbohydrate binding domains is a type of cooperative interaction that can contribute to explain some functions of modular proteoglycans in general. From our results it can be deduced that the binding strength/surface area between two aggregation factor molecules is comparable with that of focal contacts in vertebrate cells, indicating that strong carbohydrate-based cell adhesions evolved at the very start of Metazoan history.

Specific carbohydrate-carbohydrate interactions are rarely reported in biologically relevant situations such as cell recognition (1). However, carbohydrate structures have immense structural diversity (2), a ubiquitous distribution in vertebrate and invertebrate tissues (3), and are associated with the cell surface (4, 5), as required of cell recognition molecules. Carbohydrate-carbohydrate interactions are characterized by relatively weak forces that, when multimerized, can be easily potentiated by orders of magnitude, representing a highly versatile form of cell adhesion given the extraordinary plasticity of their structures (6). Among the few known examples of carbohydrate self-recognition proposed to be specific in biological processes are the multivalent binding of Lewis[x] epitopes involved in the first steps of embryogenesis (7, 8), glycolipid-glycolipid interactions controlling cell adhesion, spreading, and motility (9–11), and self-interactions of the glycan portion of sponge proteoglycans leading to species-specific cell adhesion (12, 13).

Sponge cells associate in a species-specific process through multivalent interactions of carbohydrate structures on a type of extracellular proteoglycan termed aggregation factor (14–16). Based on their molecular structure, aggregation factors have been related to hyalectans (15): large, extracellular aggregating modular proteoglycans. However, unlike hyalectans, aggregation factors do not possess common glycosaminoglycans; instead, they have complex and repetitive acidic carbohydrate motives different from those found in classical proteoglycans and mucins (17), which include novel acid-resistant and acid-labile carbohydrate domains, large and branched pyruvylated oligosaccharides (18), and other previously unknown structures (16, 19–21). In the marine sponge *Microciona prolifera* the proteoglycan molecule, *Microciona* aggregation factor (MAF[3]; $M_r = 2 \times 10^7$; Fig. 1*A*), binds cell membrane receptors via Ca^{2+}-independent interactions of small 6-kDa glycans (g6) on a 400-kDa protein (MAFp4) that corresponds to one MAF "arm" (Fig. 1*B*). Larger 200-kDa glycans (g200), bound to each of the ~20 units of the MAFp3 protein that forms the ring of MAF, self-interact through calcium-dependent associations (Fig. 1*C*). This model has been demonstrated using cell-free techniques that include bead aggregation experiments (12, 16, 22), membrane blot assays (23, 24), and force spectroscopy studies (12, 25). Recent data have shown that the binding forces recorded between g200 from the same species were significantly stronger than those observed between g200 from different species (12, 13), indicating that the measurement of adhesive forces mediated by surface glycans may contribute to the study of molecular systems having determinant implications in cellular recognition. Single-molecule force spectroscopy approaches have successfully dealt with other investigations related to cell adhesion molecules in general (26–29) and to polysaccharide interactions in particular (30–33).

MAF has been found to be polymorphic in both its protein and carbohydrate moieties, and different individuals within the species possess allotypic forms of the molecule (34). This raises the question of whether

* This work was supported in part by Grants BIO2002-00128 and BIO2005-01591 (both to X. F.-B.) from the Ministerio de Educación y Ciencia, Spain, which included Fondo Europeo de Desarrollo Regional funds. The costs of publication of this article were defrayed in part by the payment of page charges. This article must therefore be hereby marked "*advertisement*" in accordance with 18 U.S.C. Section 1734 solely to indicate this fact.

[1] Recipient of a fellowship from the Departament d'Universitats, Recerca i Societat de la Informació (Generalitat de Catalunya, Spain).

[2] Holder of Ramón y Cajal tenure track position from the Ministerio de Educación y Ciencia, Spain. To whom correspondence should be addressed: Research Center for Bioelectronics and Nanobioscience, Barcelona Science Park, Josep Samitier 1-5, Barcelona E-08028, Spain. Tel.: 34-93-403-7180; Fax: 34-93-403-7181; E-mail: xfernandez_busquets@ub.edu.

[3] The abbreviations used are: MAF, *Microciona* aggregation factor; AFM, atomic force microscope; CMF, calcium- and magnesium-free artificial seawater; CSB, chondroitin sulfate B; g6, 6-kDa glycan; g200, 200-kDa glycan; nN, nanonewton; pN, piconewton; SPR, surface plasmon resonance.

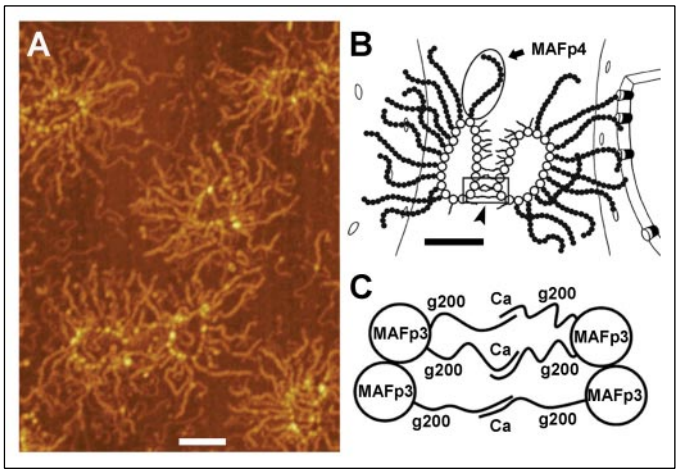

FIGURE 1. **Molecular structure of MAF.** *A*, high resolution AFM image of native MAF. The *color-coded vertical z scale* is 3 nm. *B*, schematic view of the current model depicting the interaction of two MAF molecules with the membrane receptors on two sponge cells and the MAF self-interaction through the g200 glycan. To simplify the model, only half of MAFp4 and of g200 chains are represented in each molecule. An *encircled* single MAFp4 protein unit is indicated by the *arrow*. The *arrowhead* indicates a part of the structure enlarged in *C*. *Bar*, 100 nm. *C*, schematic view of the molecular basis of MAF self-binding showing g200 chains covalently linked to the MAFp3 protein and self-interacting in a calcium-dependent process.

the species-specific carbohydrates could also have individual-specific structures and interactions, particularly in view of the fact that allotype rejection could be shown in this lowest extant Metazoan phylum (35, 36). To explore that issue, we have performed force spectroscopy and surface plasmon resonance (SPR) studies of the self-interactions of MAF and MAF subunits purified from different individual sponges. Dissecting MAF into its active adhesive components has allowed us to track the individual self-binding units down to the circular core of the sunburst-like molecule and further down to the g200 glycan itself. The identification of different allelic-like g200 forms suggests a role for carbohydrate-carbohydrate interactions in sponge allogeneic recognition. The results obtained reveal surprisingly high forces and selectivity for this most ancient cell adhesion system and open new perspectives on proteoglycan function-structure relationships.

EXPERIMENTAL PROCEDURES

Preparation of Samples and Biochemical Analyses—Specimens of the marine sponge *M. prolifera* were collected by the Marine Resources Department at the Marine Biological Laboratory in Woods Hole. Isolation of cell surface proteoglycans and purification of the g200 glycan were performed as described previously (37). g200 stock solutions were prepared by dissolving ≥10 mg of the purified lyophilized molecule in water. Calcium- and magnesium-free artificial seawater (CMF: 20 mM Tris, pH 7.4, buffered Ca^{2+}-, Mg^{2+}-free artificial seawater) was made according to the standards of the Marine Biological Laboratory (see www.mbl.edu). MAF rings were prepared according to established protocols (14). SDS-PAGE, Alcian blue stainings, Western blots, and restriction fragment length polymorphism analysis were done as described previously (35).

Atomic Force Microscope (AFM) Imaging and Force Spectroscopy—AFM visualization in air of proteoglycans was done as specified elsewhere (24). Force spectroscopy studies were performed with a Molecular Force Probe one-dimensional microscope (Asylum Research, Santa Barbara, CA). Gold-coated pyramidal Si_3N_4 tips mounted on triangular 100-μm long cantilevers (k = 0.09 newtons/m) were purchased from Olympus (Tokyo, Japan). The spring constant of every tip was measured individually through the equipartition theorem using the thermal noise of the cantilever (38) with an absolute uncertainty of ~10%. For the preparation of gold surfaces we followed the template-stripped gold method (39). The biomolecules were attached through their endogenous sulfate groups to gold-coated surfaces and tips by overlaying the surface with or floating the tip on a drop of a solution of the molecule (1 mg/ml for chondroitin sulfate B (CSB) and 0.1 mg/ml for MAF, rings, and g200) in the corresponding solvent (CMF + 2 mM $CaCl_2$ for MAF and H_2O for all others) for 1 h, followed by a wash with the respective solvents. Tips so prepared were used immediately and performed well for up to 24 h when washed with deionized H_2O and kept dry at 4 °C. Surfaces were stored by floating them on CMF + 2 mM $CaCl_2$, at 4 °C, and in these conditions they yielded reproducible results for up to 96 h.

For pulling experiments, the gold surface was mounted in the AFM and overlaid with 100 μl of CMF +10 mM $CaCl_2$. The cantilever was manually lowered to the surface, and the AFM was operated such that it moved away from and then toward the sample surface during the course of each pull. Between consecutive pulls the tip was allowed a surface dwell time of 1 s. All of the results presented here were obtained with a pulling velocity of 1 μm/s. For data analysis we used the software provided by the AFM manufacturer (IgorPro version 4.09A, WaveMetrics, Inc.). Peaks were selected manually setting a minimum length threshold of 40 nm and considering only the last adhesion event of force-extension curves except where otherwise indicated. Force peaks below 100 piconewtons (pN) were rare, and thus this value was generally chosen as lower force threshold. Calculations done automatically with different minimum force thresholds between 0 and 100 pN gave results essentially identical to those of the manual analysis. Curves that extended beyond the expected contour length of two fully stretched interacting molecules and force peaks above 1 nanonewton (nN) were not considered, and experiments containing more than 1% of either were discarded.

Exceptionally, for data analysis of control experiments we considered all force peaks regardless of their intensity or distance from the contact point. This was justified because the adhesion of the immobilized molecules to gold results in a large peak above 1 nN and less than 40 nm from the contact point. For statistical treatments the Origin 6.0 software package was used. p values were calculated with the Mann-Whitney test. As a consequence of the uncertainty inherent to the cantilever calibration described above, changing the AFM tip between two consecutive experiments might result in significant quantitative variations (up to ±10%) in the mean binding force recorded between any given pair of molecules, whereas changing only the surface did not have such an effect. For this reason p values were calculated always for the comparison of data from consecutive experiments where the tip was maintained and only the surface was changed.

SPR Studies—SPR studies were carried out with a BIAcore 1000 instrument (BIAcore AB, Uppsala, Sweden) using plain gold surfaces in Au sensor chips. When the surface was functionalized with ligand before docking the chip into the SPR system, this was done by depositing on the gold surface of the sensor 40 μl of a solution of the molecule (1 mg/ml for CSB and 0.1 mg/ml for MAF and g200) in the corresponding solvent (CMF + 2 mM $CaCl_2$ for MAF and water for g200 and CSB), followed by an overnight incubation at 4 °C in a wet chamber. Before docking the chip was washed extensively with the same solvent in which it was incubated. For each assay 60 μl of analyte solution was injected with a flow of 5 μl/min.

RESULTS

Single-molecule Force Spectroscopy of Native MAF Reveals the Existence of Multiple Intermolecular Binding Sites—MAF was bound to gold-coated surfaces and AFM tips by deposition of a 0.1 mg/ml solution of

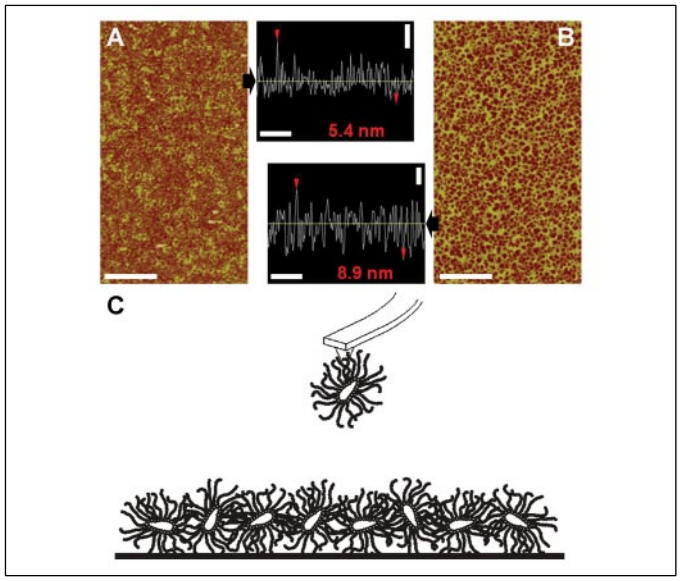

FIGURE 2. **Surface covering analysis.** AFM images of gold surfaces that have been overlaid with MAF solutions at 0.1 (*A*) and 0.2 mg/ml (*B*), extensively washed with deionized H_2O, and finally dried under N_2 flow prior to visualization are shown. The *arrows* lead to graphs showing representative 5-μm long topographic profiles of each sample. Below each profile is given the maximum vertical distance between the highest and lowest points indicated by the *arrowheads*. In force spectroscopy experiments we worked at a molecular concentration that would provide a monolayer like that in the image of *A*. The *color-coded vertical z scale* is 10 nm (*A*) and 15 nm (*B*). *Horizontal bar*, 1 μm; *vertical bar*, 2 nm. *C*, illustration of the tip and surface functionalized with MAF. For clarity, the molecules are shown standing up instead of flat on the surface.

the molecule in CMF supplemented with 2 mM Ca^{2+} (CMF + 2 mM Ca^{2+}). Binding is provided by the affinity for gold of the sulfate groups present on both g6 and g200 (12). Sponge cell aggregation experiments have shown that MAF purified from sulfate-depleted cells had an aggregative activity identical to that of sulfated MAF (40), indicating that sulfate groups are not involved in MAF self-binding and thus can be confidently used to immobilize the molecule on surfaces without affecting the functional groups. Sulfate accounts for about 4% of MAF by weight (40), an amount similar to that found in glycosaminoglycans such as CSB (41). At the concentration and incubation time used MAF covered the gold surface with a film ~5 nm thick (Fig. 2*A*), consistent with the deposition of a single layer of proteoglycans spread out and flat, in agreement with the molecular dimensions shown in Fig. 1*A*. Incubation with a 0.2 mg/ml MAF solution for an equal time resulted in the deposition of a layer about twice as deep (Fig. 2*B*), but the surface covering was not improved. Schematically, the setup for our force spectroscopy experiments is depicted in Fig. 2*C*. For clarity, in the illustration we have represented the molecules standing up. Although most likely several molecules are bound to the tip we assume that on average only one will be participating in the interaction because of the respective mean radii (~200 nm for MAF and <40 nm for the tip apex). According to the surface molecular density estimated from Fig. 2*A* (about 30 MAF/μm^2), the molecule on the tip can be expected to interact simultaneously with up to 6 MAF molecules on the surface.

Single-molecule force spectroscopy experiments performed in this way in CMF supplemented with 10 mM Ca^{2+} (CMF +10 mM Ca^{2+}) yielded curves with a sawtooth profile (Fig. 3*A*) consistent with the existence of multiple intermolecular binding sites in MAF interactions (25). When all of the force peaks are recorded they group around a maximum below 400 pN, with virtually no peaks beyond 800 pN (Fig. 3*B*). In controls done with unfunctionalized tips *versus* functionalized surfaces (Fig. 3*C*) or vice versa (not shown), force curves exhibited a completely different profile dominated by a strong short range interac-

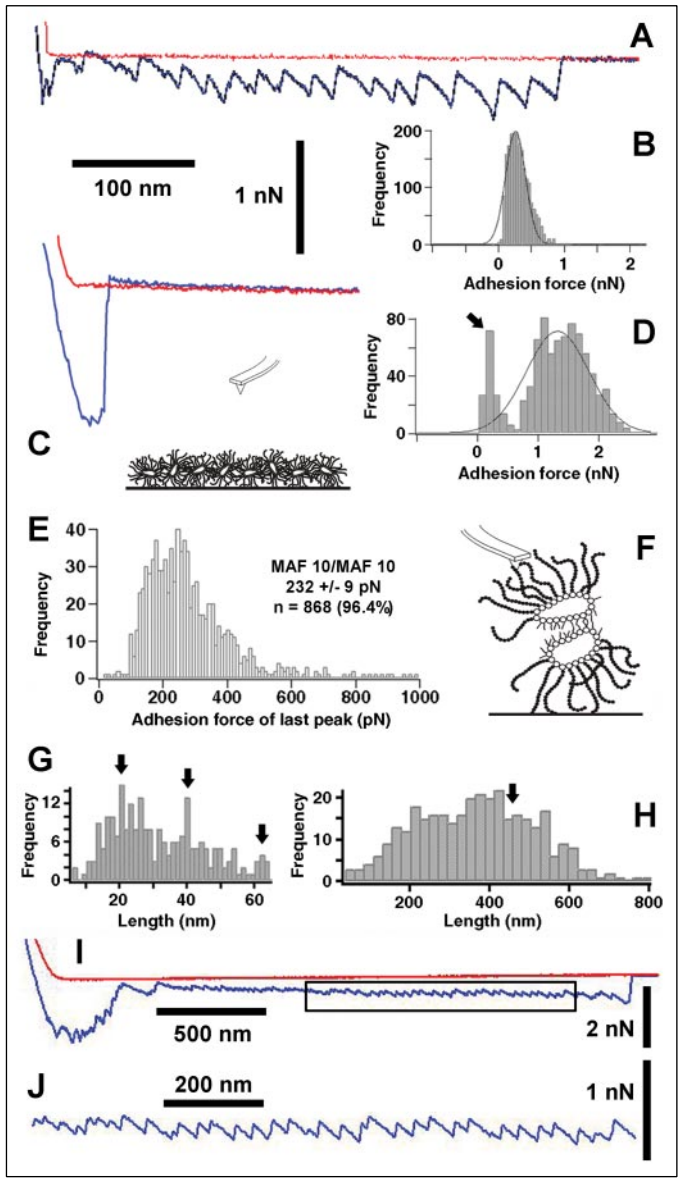

FIGURE 3. **Force spectroscopy analysis of the interaction of native MAF molecules in CMF + 10 mM Ca^{2+}.** *A*, typical profile of a MAF single-molecule self-interaction curve obtained in approach (*red*)/retract (*blue*) cycles. *B*, histogram representation of the adhesion forces for all the peaks in MAF force-extension curves from a single experiment. *C*, schematic setup and characteristic force-extension control curve showing the big adhesion peak resulting from the interaction of MAF molecules with a bare gold-coated tip. *D*, histogram representation of the adhesion forces for all the peaks in a control experiment like that of *C*. The *arrow* indicates a subset of values corresponding to MAF-MAF interactions that most likely arise when the tip picks up a MAF molecule from the surface. The complementary control experiment where a MAF-functionalized tip is tested against a bare gold surface yields essentially an identical result (not shown). *E*, histogram representing the occurrence of interaction forces in pN for the last binding events of MAF self-adhesion curves in a single experiment. We provide information about the individual from which the molecules were purified (individual 10 for this figure), the mean force value (in pN), the number of last adhesion peaks selected (*n*), and the binding probability (in percent; fraction of force curves showing adhesion events). *F*, scheme depicting the expected topography in force spectroscopy experiments of the interacting MAF molecules according to their known structure. The drawing is consistent with Fig. 1*B*, where the g200 glycan bound to MAFp3 in the ring carries the active self-binding site. The situation shown would correspond to the end of a force-extension curve where two molecules have been partially pulled off the surface and tip during stretching. *G*, histogram representing the distances between consecutive peaks in MAF force-extension curves. *Arrows* indicate three maxima at about 20, 40, and 60 nm. *H*, histogram representing the length of MAF force-extension curves in a single experiment. The *arrow* indicates the length of the curve in *A*. *I*, MAF force-distance curve obtained with a high concentration of MAF on the surface, which results in the pulling of several molecules in a string. *J*, enlargement of the retracting curve section *boxed* in *I*.

tion that reflects the binding of MAF to gold (see force-extension curve in Fig. 3*C*). A histogram representation shows the corresponding Gaussian fit centered at ~1.3 nN and spreading well beyond 2 nN (Fig. 3*D*), in good agreement with the reported strength of a sulfur-gold bond (42). The smaller peak indicated by the *arrow* in Fig. 3*D* is attributed to MAF-MAF interactions resulting from molecules that are being ripped off the surface by the gold tip that in this way becomes also functionalized. Rather than visualizing a good surface covering we have chosen as the best control for all the experiments presented in this work the presence of a histogram representation like that in Fig. 3*B*, lacking the characteristic interaction with gold above 1 nN. Controls were also performed with the objective of blocking any gold surface that could have remained exposed and that might interfere with the MAF self-binding. This was done immediately after MAF deposition by extensively washing away unbound proteoglycan with CMF + 2 mM Ca^{2+} and overlaying the surface for 30 min with a solution of 6 mg/ml L-cysteine in a buffer containing 1 M NaCl and 0.1 M formate, pH 4.3 (43). The resulting force curves were indistinguishable from those obtained in the absence of the blocking step, and therefore the simplest and less aggressive method (*i.e.* without blocking) was chosen.

The last peak of each pull was similar to all previous peaks in the same curve (Fig. 3*A*), as expected from an intermolecular polyvalent adhesive interaction. A significantly stronger last peak might reflect the detachment of molecules from the gold surface. The binding efficiency was very high, with more than 95% of approach-retract cycles resulting in adhesion, thus confirming a good surface coverage and the adequate preservation of the activity of the immobilized molecules. To ensure measuring only truly adhesive interactions, data collection from intermolecular adhesion experiments was restricted to the last peak of force curves except where otherwise indicated. The mean forces measured for this last adhesion event varied depending on the individual origin of the molecules between 200 and 300 pN (232 ± 9 pN for the example of Fig. 3*E*).

If the force peaks obtained resulted from g200-g200 interactions and if, as deduced from biochemical evidence, g200 is on the ring of MAF (24) (Fig. 3*F*), the distance between peaks in a curve should correspond to the distance between g200 attachment points in the ring of the molecule. When the distance between consecutive peaks in MAF force-extension curves is computed, the resulting graph shows maxima at about 20, 40, and 60 nm (Fig. 3*G*). The observation that 20 is the most abundant value and that 40 and 60 are multiples of it (thus probably resulting from missing peaks rather than from the real spacing between anchoring points) suggests that g200 attachment sites are about 20 nm apart. From good resolution AFM images of MAF taken in air the spacing between g200 glycans on the ring was calculated to be 14 ± 2 nm (24). This discrepancy might reflect a more extended configuration of the molecule in liquid and/or the existence of elastic phenomena that are manifested in force spectroscopy experiments (44).

The length of the curves showed a wide distribution up to ~800 nm (Fig. 3*H*), and the number of peaks in a curve seldom exceeded 20, in agreement with interactions of a single molecular pair according to the known dimensions and structure of MAF. Short force-extension curves likely result from interactions between molecules bound tightly to surface and tip, whereas the longest pulls must arise from contacts between molecules that have fewer connections to gold and therefore can be partially lifted during extension. Force curves obtained after deposition on the gold surface of more concentrated MAF solutions (>0.2 mg/ml) could reach a length of several microns (Fig. 3*I*). These long curves maintained the typical jagged profile (Fig. 3*J*) and are the consequence of pulling concatamers made up of several MAF molecules. After hundreds of cycles the sawtooth pattern of the curves remained unaltered, indicating repeated zipping and unzipping of the intermolecular bonds.

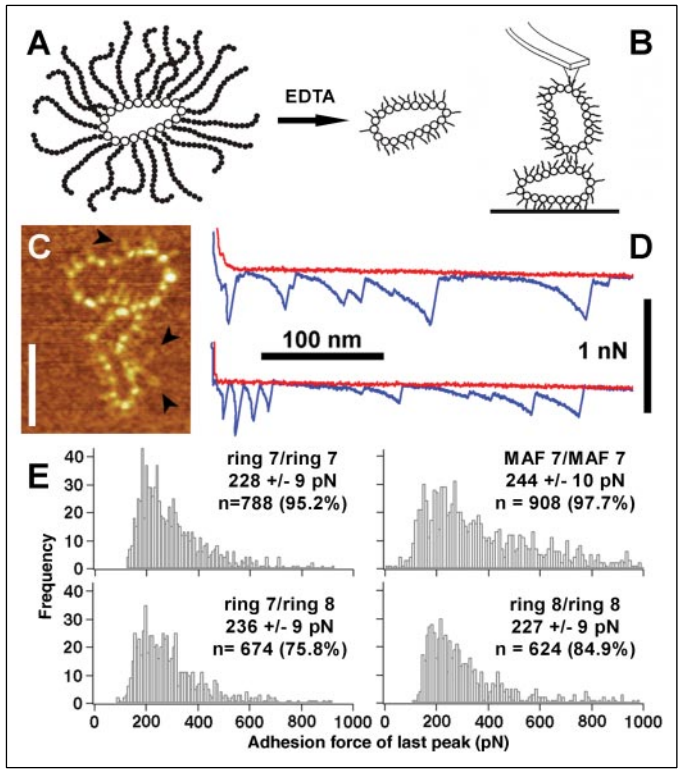

FIGURE 4. **Force spectroscopy analysis of the interaction of MAF rings in CMF + 10 mM Ca^{2+}.** *A*, schematic representation of the process of elimination of MAF arms through incubation with EDTA. *B*, scheme of the experimental setup for ring force spectroscopy measurements. For clarity, the molecules are shown standing up instead of flat on the surface. The situation shown would correspond to the end of a force-extension curve where two molecules have been partially pulled off the surface and tip during stretching. *C*, high resolution AFM image of MAF rings. *Arrowheads* indicate g200 chains linked to MAFp3 protein subunits in the ring. The *color-coded vertical z scale* is 3 nm. *Bar*, 100 nm. *D*, characteristic profiles of ring self-interaction curves obtained in approach/retract cycles. *E*, histograms representing the occurrence of adhesion forces in pN for the last binding events of curves of isotypic MAF (*7/7*) and ring (*7/7 and 8/8*) and of allotypic ring interactions (*7/8*).

The arms of MAF have a modular structure resulting from the presence of a multiplicity of globular domains (15, 24), and the shape of MAF force-extension curves could also be consistent with the unfolding of such intramolecular protein domains (45). To explore this possibility, force spectroscopy experiments had to be performed with MAF molecules devoid of arms.

Single-molecule Force Spectroscopy of MAF Ring Interactions—The arms of MAF, representing about three-fourths of the total mass of the molecule (24), can be easily eliminated by removing calcium from the medium with a treatment in the presence of 1 mM EDTA (14) (Fig. 4*A*). AFM imaging on mica of ring preparations reveals a characteristic beaded appearance (Fig. 4*C*), where each of the ~20 beads in a ring is a MAFp3 unit (24). In hyalectans, the glycosylated link protein interacts with the proteoglycan monomer core protein, which is heavily substituted with glycosaminoglycan chains. In MAF, each glycosylated MAFp3 interacts with one arm that corresponds to the glycosylated MAFp4 protein (15). Despite the topological analogy of MAFp3 and the hyalectan link protein, their amino acid sequences do not have significant homology. In high resolution AFM images, structures supposed to represent g200 can be seen as one or two short chains up to 30 nm long protruding from the MAFp3 beads (Fig. 4*C*, *arrowheads*).

The resulting ring preparations yield reproducible force-distance curves in single-molecule force spectroscopy experiments performed in

CMF + 10 mM Ca^{2+} (Fig. 4, *B* and *D*). The maximum length of ring pulls is ~300 nm, again in good agreement with single-pair interactions when considering the known structure of the molecule (24). Compared with intact MAF, the pattern of peaks obtained with ring preparations was not as regularly spaced, and the mean distance between peaks was longer, most likely because in the absence of the sulfated g6 glycan present on the MAF arms many of the g200 sulfate groups are now recruited for the binding to the gold surface, thus imposing a constraint on the freedom of g200 to interact. The force recorded for the last adhesion peak in ring interactions was about 10% smaller than that obtained with the native molecule from the same individual (Fig. 4*E*, compare histograms *MAF 7/MAF 7* with *ring 7/ring 7*). This small difference is within the uncertainty margin of cantilever calibration, and thus it cannot be considered significant. The overall shape of the curves and the maintenance of the binding force represent the first direct evidence that g200 is located in the ring of the molecule.

Given the variation mentioned above in binding force between MAF molecules of different individual origin, we decided to investigate whether glycan adhesion forces could be acting in the discrimination of isotypic (between MAF from the same individual) *versus* allotypic (between MAF from different individuals) molecule contacts. If so, one would expect to find differences when comparing the adhesion of isotypic *versus* allotypic combinations in force spectroscopy experiments. For ring interaction assays, we purified MAF from two sponge individuals, as assessed by restriction fragment length polymorphism analysis (not shown). Mean binding forces for isotypic ring interactions 7/7 and 8/8 (228 and 227 ± 9 pN, respectively) did not significantly differ from the allotypic 7/8 (236 ± 9 pN) (Fig. 4*E*), and *p* values for the difference in binding force between ring isotypic and allotypic interactions were not significant (generally >0.05). However, our polymorphism assays are based on DNA sequences of the MAF proteins MAFp3 and MAFp4, which had been shown to be good individual markers (34), but they do not provide information about the existence of different g200 allotypic forms in the specimens under study. This requires the purification of g200 and the direct analysis of the glycan.

Force Spectroscopy Analysis of Allotypic versus Isotypic g200 Glycans—Preexisting immunochemistry data suggested that the variability of MAF resided also in g200 (44). g200 is a complex glycan containing fucose, glucuronic acid, *N*-acetylglucosamine, galactose, and mannose, which can be purified by extensive Pronase digestion of MAF followed by size exclusion chromatography (16) (Fig. 5*A*). When analyzed in SDS-PAGE, g200 preparations of different individual origin exhibited bands with different mobilities, which recalled the presence of discrete alleles (Fig. 5*C*). In four individuals examined (labeled 2–5) we found three different g200 sets according to electrophoretic mobility: individual 4 having what we named allele *a*, individual 5 with allele *b*, and individuals 2 and 3 apparently harboring *a* and *b* (only 3 is shown). Immunoblot results obtained with the monoclonal antibody Block 2, raised against a sulfated disaccharide epitope present in g200 which is involved in its self-interaction (16, 20), indicated that the system is more complex: g200 forms with similar electrophoretic mobilities contain highly differing amounts of the sulfated epitope (Fig. 5*D*, allele *a* in individuals 3 and 4 and allele *b* in individuals 3 and 5).

Together with preliminary analyses of nonpurified g200 (15), our data based on electrophoretic mobility indicate that a single sponge individual usually contains one or two forms of the glycan. g200 force spectroscopy experiments were performed in CMF + 10 mM Ca^{2+} with the allelic forms *a* and *b*, allowing us to make comparative adhesion studies between isotypic and allotypic g200 self-interactions. The close spacing between peaks in g200 adhesion curves (Fig. 5*E*) likely reflects interactions between several glycan molecules on both tip and surface as a consequence of the random distribution of g200 on the gold surfaces. Such patterns were never observed in the experiments done with native

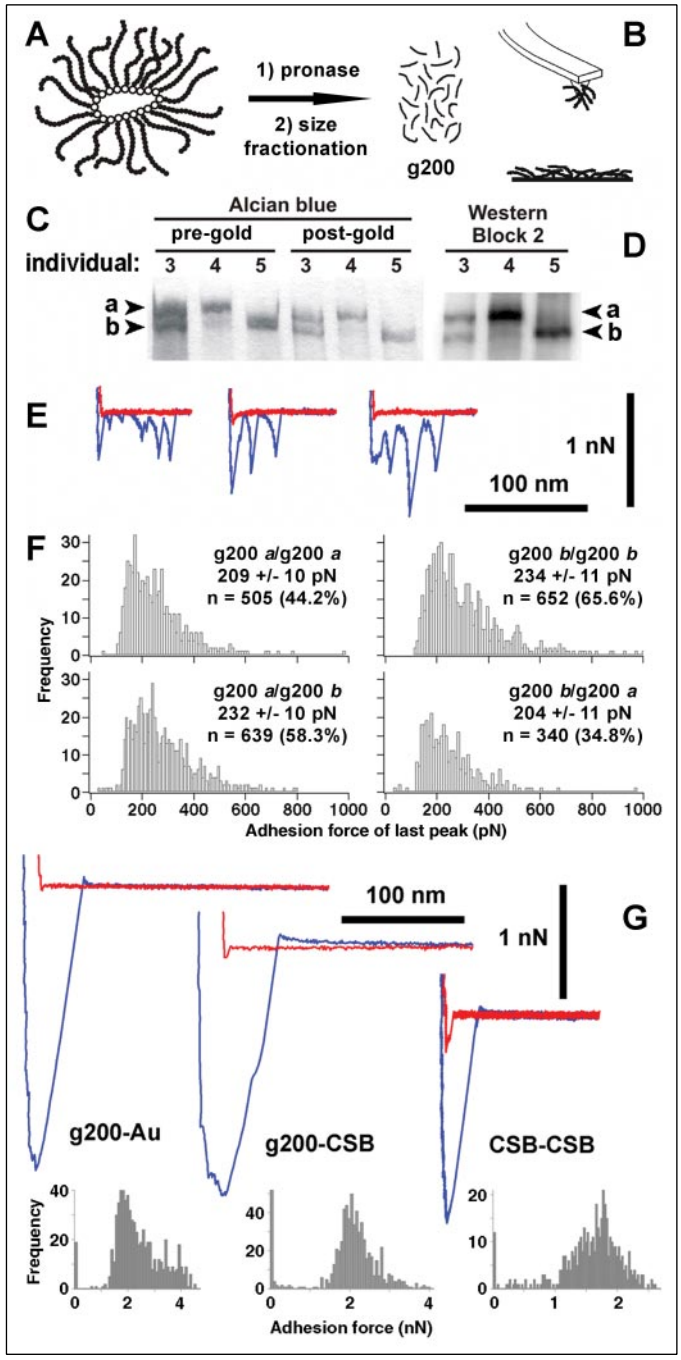

FIGURE 5. **Force spectroscopy analysis of the g200 self-interaction in CMF + 10 mM Ca^{2+}.** *A*, schematic representation of the process of purification of g200. The location of g200 within MAF is shown in Fig. 1*B*. *B*, scheme of the experimental setup for g200 force spectroscopy measurements. *C*, Alcian blue staining of g200 purified from three different individuals (*3*, *4*, and *5*) electrophoresed in a 5% SDS-polyacrylamide gel. Equal volumes of each sample were loaded before (*pre-gold*) and after (*post-gold*) deposition on the gold surfaces used in force spectroscopy assays. *D*, Western blot of the same g200 preparations decorated with Block 2. The amounts loaded in each lane were one-tenth of the pre-gold samples from *C*. *E*, three representative g200 self-interaction curves obtained in approach/retract cycles. *F*, histograms representing the occurrence of adhesion forces in pN for the last binding events of curves of isotypic (*a/a* and *b/b*) and allotypic g200-g200 interactions (*a/b* and *b/a*). In allotypic combinations the first sample was bound to the tip and the second sample to the surface. *G*, characteristic profiles of interaction curves obtained in approach/retract cycles for the controls *g200-Au*, *g200-CSB*, and *CSB-CSB* and the corresponding histogram representations of all peaks in three separate experiments.

MAF and only occasionally in the experiments done with rings (Fig. 4*D*, *lower curve*), probably because of the regular spacing between g200 attachment points as long as the ring of MAF remains intact. The maximum length of g200-g200 pulls was ~60 nm, consistent with high resolution AFM images taken in air where the length of g200 was estimated to be ~30 nm (24).

The average force recorded for the last adhesion peak in isotypic g200 force-extension curves (~209 and ~234 pN, for *a-a* and for *b-b* respectively; Fig. 5*F*) is not too much different from the values obtained in the experiments performed with native MAF and with rings, indicating that the procedure used to prepare g200 did not significantly modify the binding properties of the glycan. The mean adhesion forces for allotypic *a-b* interactions (or the control *b-a*, where the molecular species bound to tip and surface were used in the reverse combination) did not differ significantly from those of isotypic *a-a* and *b-b*. However, *p* values for the difference in adhesion force between g200 isotypic and allotypic interactions were significant (<0.05).

In CMF + 10 mM Ca^{2+} the measured interaction between a g200-derivatized tip and a gold surface was strong and of short range (below 40 nm, Fig. 5*G*), reflecting the binding of g200 sulfate groups to gold, which we use as immobilization strategy. Efficient binding of g200 to gold was further assessed by an independent approach that consisted of the electrophoretic analysis followed by Alcian blue staining of a g200 solution before and after its incubation on gold surfaces (Fig. 5*C*), which confirmed that post-gold solutions always contained significantly less g200 than pre-gold solutions. Most adhesion curves in force spectroscopy experiments of the interaction between g200 and an unrelated sulfated glycan of similar size such as CSB (mean size 150 kDa compared with 200 kDa for g200) had a profile completely different from that of g200-g200 interactions shown in Fig. 5*E*, lacking the typical 200–300 pN peaks and being dominated by an apparently unspecific short range interaction similar to that recorded for g200-gold and for CSB-CSB interactions (Fig. 5*G*). Such a result could be explained as the consequence of a very poor adhesion between g200-CSB and CSB-CSB which would facilitate the interaction of the immobilized molecules with the underlying gold surface. To characterize further this apparently weak binding we have studied the g200-CSB interaction by SPR.

SPR Study of g200-g200 and of g200-CSB Binding at 2 mM Ca^{2+}—SPR experiments attempted in the presence of 10 mM Ca^{2+} failed because of clogging of the channel system by self-aggregating g200. At 2 mM Ca^{2+} massive self-aggregation was not detected, and this concentration still allowed us to characterize the g200-CSB interaction by SPR. In the absence of Ca^{2+}, 0.1 mg/ml g200 binds to the gold surface of the SPR chip (Fig. 6*A*), whereas 1 mg/ml CSB added to the g200-functionalized gold surface does not show significant binding. The level of immobilized ligand was around 1,000 response units, an appropriate value for kinetic measurements (43). When the order of addition is reversed (Fig. 6*B*), CSB binds to the gold surface, although with slower kinetics than g200, even at a concentration 10 times higher than that of g200. However, this control indicates that if there is binding of soluble CSB analyte to the immobilized g200 ligand, it can be detected by SPR.

In CMF + 2 mM Ca^{2+} g200 binds to a g200-functionalized surface (Fig. 6*C*), presumably by self-aggregating until the multilayer that forms reaches an equilibrium with its dissociation. CSB added at this point does not bind to g200, although if more g200 is added further binding is again recorded. These SPR results confirm a specific self-binding of g200, which readily interacts with itself, but not with an unrelated sulfated glycan such as CSB. The measured binding of g200 is of about 1,400 response units, far below the maximum expected figure for a 200-kDa molecule, which can give results up to 20,000 response units

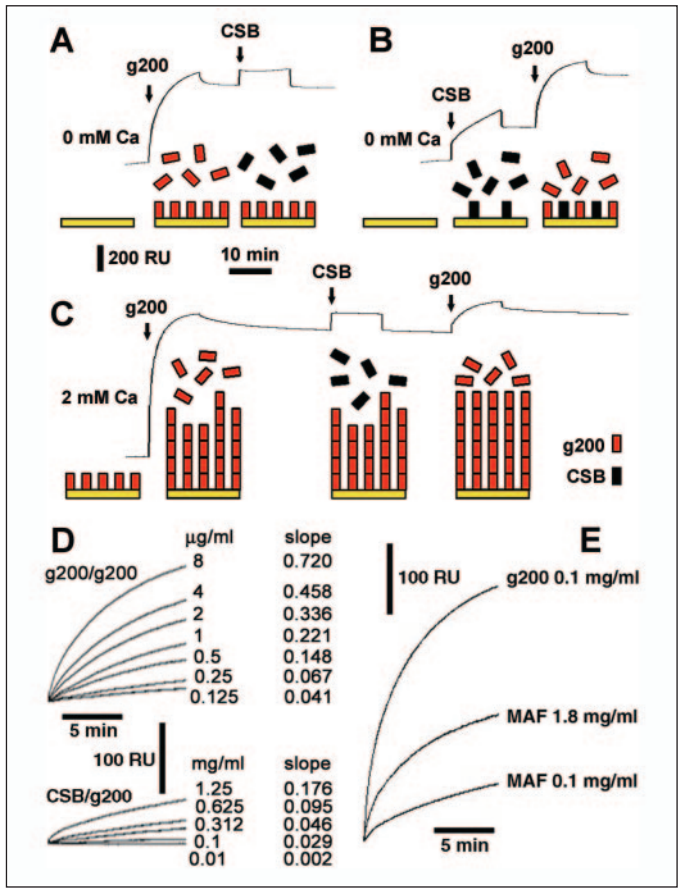

FIGURE 6. **SPR analysis of the interaction g200-CSB.** *A*, g200 dissolved in water was added to a plain gold SPR chip, and binding was recorded. The accompanying illustrations show the successive steps. After an elution time, CSB dissolved in water was added to the same channel. *B*, in a second channel, the same solutions as in *A* were added in reverse order. *C*, in a third channel where g200 had been immobilized previously as in *A*, g200 and CSB dissolved in CMF containing 2 mM Ca^{2+} were alternatively injected, each injection separated by adequate elution times. g200 and CSB concentrations in *A–C* were always 0.1 and 1 mg/ml, respectively. The steep jumps at the beginning and end of CSB injections are bulk effects caused by the high analyte concentration and are not related to interactions with the surface. *D*, the gold surface of a SPR chip that had been overlaid for 12 h with a 0.1 mg/ml solution of g200 was flushed with growing concentrations of g200 (*g200/g200*, from 0.125 to 8 µg/ml) and of CSB (*CSB/g200*, from 0.01 to 1.25 mg/ml) in CMF + 2 mM Ca^{2+}. Slope values correspond to the 1st min of the binding curves. *E*, the gold surface of a SPR chip that had been overlaid for 12 h with a 0.1 mg/ml solution of MAF was flushed with MAF (0.1 and 1.8 mg of carbohydrate/ml) or with 0.1 mg/ml g200 in CMF + 2 mM Ca^{2+}, each sample in a different channel. *RU*, response units.

before reaching the limit of detection by the SPR system (43), which is affected by interactions within about 300 nm of the surface (46). This upper limit depends on the ligand covering of the chip surface and on the affinity of the interacting molecules. In control experiments where cysteine was used to block any gold surfaces exposed after g200 deposition (43), the results were equivalent to those obtained without this blocking step (data not shown), indicating that the g200 layer efficiently covered the chip surface. However, because at a calcium concentration of 2 mM MAF does not aggregate sponge cells, it is likely that the g200 interactions that take place in this condition are relatively weak, contributing to the low SPR response.

To obtain a g200 covering as complete as possible, the surface of a gold chip was overlaid for 16 h with a 0.1 mg/ml solution of g200. Detailed SPR analysis on a g200-functionalized surface prepared in that way (Fig. 6*D*) indicated that in the presence of 2 mM Ca^{2+} there is a basal binding between g200 and CSB, about 3 orders of magnitude weaker than the recorded g200 self-adhesion at the same calcium concentration. Self-binding of CSB to a CSB-functionalized SPR gold surface in

the presence of 2 mM Ca^{2+} was insignificant (not shown) and comparable with the weak affinity of CSB for g200, in agreement with our force spectroscopy results.

In force spectroscopy experiments, the adhesion force recorded in the peaks of g200-g200 interactions was comparable with that from MAF force-extension curves. As discussed above, we therefore deduced that g200 carried the active self-binding site. If so, purified g200 should strongly interact with a MAF-functionalized SPR surface. Indeed, a 0.1 mg/ml solution of g200 binds much more efficiently than a 0.1 mg of carbohydrate/ml of MAF solution to a MAF-derivatized SPR surface in 2 mM Ca^{2+} (Fig. 6*E*). Because g200 represents by mass about one-half of total MAF carbohydrate, we repeated the experiment with a higher amount of soluble MAF analyte (1.8 mg of carbohydrate/ml, which contains ~0.9 mg of g200/ml). Even at this concentration, the binding of intact MAF is much less than the binding of g200 at 0.1 mg/ml.

DISCUSSION

Force-extension curves of MAF self-interactions resemble those obtained in the stretching and unfolding of a long molecule that is compacted into domains (47), as has been shown for single elastic protein molecules such as titin (45), tenascin (28), and fibronectin (27). However, force spectroscopy experiments performed with purified g200 in the absence of MAF protein yielded force peaks comparable with those observed with native MAF, indicating that the event under study is not the result of protein unfolding. Because carbohydrates are not known to fold into domains, we must conclude that the force measured in each peak reflects the breaking of an adhesive intermolecular association between a pair of g200 units. Generally, the peak maximum in MAF pulls does not increase with increasing extension, suggesting that the intermolecular bonds are not sorted in the extension curves according to their adhesion force but rather to their position on the interacting molecules, in agreement with the zipper-like model. The multiplicity of binding sites confers a high degree of modulability as required in most biological interactions, in contrast to the higher stability of a single, strong bond. This modular elongation mechanism, be it intra- or intermolecular, has been proposed to be a general strategy for conveying toughness to natural fibers and adhesives (48). MAF force extension curves, then, derive from the existence of intermolecular adhesion domains that through the summation of multiple single binding sites provide strong adhesion forces for the resulting polymer (49).

The biological roles assigned to proteoglycans are highly diversified, ranging from relatively straightforward mechanical functions to effects on more dynamic processes such as cell adhesion and motility, to complex and still poorly understood roles in cell differentiation and development (50–53). Angiogenesis, axon guidance and synapse development, metastasis, and patterning events are just some examples of processes that require finely tuned interactions between cells or between cells and the extracellular matrix where proteoglycans are involved (54–60). The cooperativity of abundant, relatively weak, intermolecular carbohydrate adhesion domains like those found in MAF might provide a molecular basis for some of the functions of modular proteoglycans.

When MAF-MAF force measurements were done in the presence of Block 2 the recorded force decreased by ~50% (25). If Ca^{2+} is lowered to 2 mM the MAF self-interaction force also drops to ~50% and the binding probability to ~25% relative to the experiments done in the presence of 10 mM Ca^{2+} (25). Our SPR data obtained in CMF + 2 mM Ca^{2+} show a steep decrease in MAF self-binding compared with g200-MAF binding, suggesting that in low calcium we might be detecting g200 adhesive properties different from those acting at 10 mM Ca^{2+}, which could be masked when g200 is buried within the environment of the native molecule. Taken together, these results indicate the participation of other interactions independent from Ca^{2+} and from the sulfated antigen epitope targeted by Block 2, as expected from the complexity of MAF glycans (17, 18). Self-recognition of g200 is not simply based on electrostatic interactions, as shown by SPR experiments where other similarly charged carbohydrates analyzed did not aggregate (46). The sulfated disaccharide self-associated in the presence of Ca^{2+}, but the interaction was completely eradicated on substitution of Ca^{2+} ions by either Mg^{2+} or Mn^{2+} ions. This is consistent with a rapid multiple low affinity event where Ca^{2+} provides not only electrostatic forces but contributes via coordinative forces to glycan superstructures (6, 46). In this scenario, simple charge effects may lead to nonspecific interactions in low calcium concentrations that might be overcome when more calcium is present, allowing the organization of sugar moieties and enhancing the adhesion between specific carbohydrate groups.

If g200 were a linear polymer it would have a length of ~180 nm (25). However, it has to be noted that g200 might have a branched structure characteristic of many complex glycans, which would significantly influence the electrophoresis and size fractionation approaches used to estimate its molecular mass (16). Actually, the fraction assigned to g200 in gel filtration experiments peaks between 200 and 40 kDa, with a maximum of absorbance at 100 kDa according to linear glycosaminoglycan molecular mass standards (16). The real mass (and the expected length) of a branched glycan with such an elution profile might be much smaller, in agreement with the short structures attributed to g200 in our AFM images. g200 does not belong to any of the main glycosaminoglycan types described in higher animals, as suggested by its elevated fucose content and its resistance to common glycosaminoglycan-digesting enzymes (16). Preliminary nuclear magnetic resonance analyses performed with intact g200 chains indicated such a structural diversity that the possible existence of a backbone containing a basic repetitive oligosaccharide unit could not be determined (21). This complex structure of g200, in contrast to the much simpler linear repetitive chains of CSB, heparan sulfate, or hyaluronan, can provide the basis for its highly selective adhesive properties in 10 mM Ca^{2+}, as illustrated by a strong intraspecies-specific binding, weaker interspecies-specific interactions (12), and very small adhesion forces with other unrelated glycosaminoglycans.

Our data reveal the existence of interindividual differences in size, epitope content, and binding forces between cell adhesion glycans. This previously undescribed allelic variability can have its basis in genetic, developmental, and environmental factors and might have essential cellular functions likely related to some aspect of sponge allogeneic recognition (61). The detailed study of tissue rejection reactions in *M. prolifera* (62) has revealed that whenever two sponge individuals mutually reject their tissues in graft experiments, they have different genomic fingerprints for the DNA sequences coding for MAF proteins (34, 35). This observation indicated a direct involvement of sponge cell adhesion molecules in histocompatibility reactions, although the corresponding mechanism has not been worked out yet. The results presented here suggest that adhesion force differences between different allelic forms of glycosaminoglycans might be a factor implicated in the initial phases of allogeneic recognition between tissues of different individual origin. To nail down this point, future studies will have to overcome the limited availability of sponge individuals of sufficient size and the long protocol used for high purification of the necessary amounts of g200, which were obstacles in extending our study to a larger number of allelic variants of the glycan.

Sponges are the most ancient extant Metazoans and therefore good

candidates to possess descendants of the primordial cell adhesion molecules that led to stable cell interactions. The first multicellular animals were likely to consist of loose assemblies of single cells forming clumps that continuously dissociated and reassociated in a random process. Next, cell surface molecules must have evolved which allowed the segregation of genetically identical cell masses, the first pluricellular individuals. Once the genetic material was so compartmented, the biological evolution of animals could speed up. Based on the known structure and dimensions of MAF, the adhesive force between two single molecules can be calculated. If we assume an interaction of only half of the ~25 g200 units present on a MAF ring, it results that the force binding two MAF molecules (about 2–3 nN) is of the same magnitude as that exerted over an area of similar size (~0.15 μm^2) in focal cellular contacts (63, 64). This unexpected result reveals that the early cell adhesion systems that allowed stable cell contacts leading to the appearance of Metazoans were based on very strong forces comparable with those holding together the tissues of present day vertebrates and that carbohydrate structures were essential components of the molecules involved.

Acknowledgments—We thank the Scientific and Technical Services of the University of Barcelona for technical assistance and Dr. Stefan Vinzelberg (Atomic Force, Germany) for help in software development.

REFERENCES

1. Bucior, I., and Burger, M. M. (2004) *Curr. Opin. Struct. Biol.* **14,** 631–637
2. Dietrich, C. P., Nader, H. B., and Straus, A. H. (1983) *Biochem. Biophys. Res. Commun.* **111,** 865–871
3. Cássaro, C. M., and Dietrich, C. P. (1977) *J. Biol. Chem.* **252,** 2254–2261
4. Hook, M., Kjellén, L., and Johansson, S. (1984) *Annu. Rev. Biochem.* **53,** 847–869
5. Roseman, S. (2001) *J. Biol. Chem.* **276,** 41527–41542
6. Spillmann, D., and Burger, M. M. (2000) *Carbohydrates in Chemistry and Biology: A Comprehensive Handbook*, pp. 1061–1091, Wiley-VCH Verlag GmbH, Weinheim, Germany
7. Eggens, I., Fenderson, B., Toyokuni, T., Dean, B., Stroud, M., and Hakomori, S. (1989) *J. Biol. Chem.* **264,** 9476–9484
8. Pincet, F., Le Bouar, T., Zhang, Y., Esnault, J., Mallet, J. M., Perez, E., and Sinaÿ, P. (2001) *Biophys. J.* **80,** 1354–1358
9. Kojima, N., and Hakomori, S. (1991) *J. Biol. Chem.* **266,** 17552–17558
10. Dicko, A., Heng, Y. M., and Boggs, J. M. (2003) *Biochim. Biophys. Acta* **1613,** 87–100
11. Wang, X., Sun, P., Al Qamari, A., Tai, T., Kawashima, I., and Paller, A. S. (2001) *J. Biol. Chem.* **276,** 8436–8444
12. Bucior, I., Scheuring, S., Engel, A., and Burger, M. M. (2004) *J. Cell Biol.* **165,** 529–537
13. Bucior, I., and Burger, M. M. (2004) *Glycoconj. J.* **21,** 111–123
14. Humphreys, S., Humphreys, T., and Sano, J. (1977) *J. Supramol. Struct.* **7,** 339–351
15. Fernàndez-Busquets, X., and Burger, M. M. (2003) *Cell Mol. Life Sci.* **60,** 88–112
16. Misevic, G. N., and Burger, M. M. (1993) *J. Biol. Chem.* **268,** 4922–4929
17. Misevic, G. N., Guerardel, Y., Sumanovski, L. T., Slomianny, M. C., Demarty, M., Ripoll, C., Karamanos, Y., Maes, E., Popescu, O., and Strecker, G. (2004) *J. Biol. Chem.* **279,** 15579–15590
18. Guerardel, Y., Czeszak, X., Sumanovski, L. T., Karamanos, Y., Popescu, O., Strecker, G., and Misevic, G. N. (2004) *J. Biol. Chem.* **279,** 15591–15603
19. Misevic, G. N., and Burger, M. M. (1990) *J. Biol. Chem.* **265,** 20577–20584
20. Spillmann, D., Thomas-Oates, J. E., van Kuik, J. A., Vliegenthart, J. F., Misevic, G., Burger, M. M., and Finne, J. (1995) *J. Biol. Chem.* **270,** 5089–5097
21. Spillmann, D., Hård, K., Thomas-Oates, J., Vliegenthart, J. F., Misevic, G., Burger, M. M., and Finne, J. (1993) *J. Biol. Chem.* **268,** 13378–13387
22. Jarchow, J., and Burger, M. M. (1998) *Cell Adhes. Commun.* **6,** 405–414
23. Popescu, O., and Misevic, G. N. (1997) *Nature* **386,** 231–232
24. Jarchow, J., Fritz, J., Anselmetti, D., Calabro, A., Hascall, V. C., Gerosa, D., Burger, M. M., and Fernàndez-Busquets, X. (2000) *J. Struct. Biol.* **132,** 95–105
25. Dammer, U., Popescu, O., Wagner, P., Anselmetti, D., Güntherodt, H. J., and Misevic, G. N. (1995) *Science* **267,** 1173–1175
26. Benoit, M., Gabriel, D., Gerisch, G., and Gaub, H. E. (2000) *Nat. Cell Biol.* **2,** 313–317
27. Oberhauser, A. F., Badilla-Fernandez, C., Carrion-Vazquez, M., and Fernandez, J. M. (2002) *J. Mol. Biol.* **319,** 433–447
28. Oberhauser, A. F., Marszalek, P. E., Erickson, H. P., and Fernandez, J. M. (1998) *Nature* **393,** 181–185
29. Zhang, X., Wojcikiewicz, E., and Moy, V. T. (2002) *Biophys. J.* **83,** 2270–2279
30. Abu-Lail, N. I., and Camesano, T. A. (2003) *J. Microsc.* **212,** 217–238
31. Tromas, C., Rojo, J., de la Fuente, J. M., Barrientos, A. G., García, R., and Penadés, S. (2001) *Angew. Chem. Int. Ed. Engl.* **40,** 3052–3055
32. Seog, J., Dean, D., Plaas, A. H. K., Wong-Palms, S., Grodzinsky, A. J., and Ortiz, C. (2002) *Macromolecules* **35,** 5601–5615
33. De La Fuente, J. M., and Penadés, S. (2004) *Glycoconj. J.* **21,** 149–163
34. Fernàndez-Busquets, X., Gerosa, D., Hess, D., and Burger, M. M. (1998) *J. Biol. Chem.* **273,** 29545–29553
35. Fernàndez-Busquets, X., and Burger, M. M. (1997) *J. Biol. Chem.* **272,** 27839–27847
36. Müller, W. E. G., and Müller, I. M. (2003) *Integr. Comp. Biol.* **43,** 281–292
37. Misevic, G. N., Finne, J., and Burger, M. M. (1987) *J. Biol. Chem.* **262,** 5870–5877
38. Florin, E. L., Rief, M., Lehmann, H., Ludwig, M., Dornmair, C., Moy, V. T., and Gaub, H. E. (1995) *Biosensors Bioelec.* **10,** 895–901
39. Hegner, M., Wagner, P., and Semenza, G. (1993) *Surface Sci.* **291,** 39–46
40. Kuhns, W. J., Popescu, O., Burger, M. M., and Misevic, G. (1995) *J. Cell. Biochem.* **57,** 71–89
41. Alberts, B., Bray, D., Lewis, J., Raff, M., Roberts, K., and Watson, J. D. (1989) *Molecular Biology of the Cell*, 2nd Ed., p. 805, Garland Publishing, Inc., New York
42. Grandbois, M., Beyer, M., Rief, M., Clausen-Schaumann, H., and Gaub, H. E. (1999) *Science* **283,** 1727–1730
43. (1994) *BIAapplications Handbook*, Pharmacia Biosensor AB, Uppsala, Sweden
44. Fritz, J., Anselmetti, D., Jarchow, J., and Fernàndez-Busquets, X. (1997) *J. Struct. Biol.* **119,** 165–171
45. Rief, M., Gautel, M., Oesterhelt, F., Fernandez, J. M., and Gaub, H. E. (1997) *Science* **276,** 1109–1112
46. Haseley, S. R., Vermeer, H. J., Kamerling, J. P., and Vliegenthart, J. F. (2001) *Proc. Natl. Acad. Sci. U. S. A.* **98,** 9419–9424
47. Carrion-Vazquez, M., Oberhauser, A. F., Fisher, T. E., Marszalek, P. E., Li, H., and Fernandez, J. M. (2000) *Prog. Biophys. Mol. Biol.* **74,** 63–91
48. Smith, B. L., Schäffer, T. E., Viani, M., Thompson, J. B., Frederick, N. A., Kindt, J., Belcher, A., Stucky, G. D., Morse, D. E., and Hansma, P. K. (1999) *Nature* **399,** 761–763
49. Misevic, G. N., and Burger, M. M. (1986) *J. Biol. Chem.* **261,** 2853–2859
50. De Cat, B., and David, G. (2001) *Semin. Cell Dev. Biol.* **12,** 117–125
51. Schwartz, N. (2000) *Front. Biosci.* **5,** D649–D655
52. Rapraeger, A. C. (2001) *Semin. Cell Dev. Biol.* **12,** 107–116
53. Kresse, H., and Schönherr, E. (2001) *J. Cell. Physiol.* **189,** 266–274
54. Yamaguchi, Y. (2001) *Semin. Cell Dev. Biol.* **12,** 99–106
55. Rauch, U., Feng, K., and Zhou, X. H. (2001) *Cell Mol. Life Sci.* **58,** 1842–1856
56. Sanderson, R. D. (2001) *Semin. Cell Dev. Biol.* **12,** 89–98
57. Blackhall, F. H., Merry, C. L., Davies, E. J., and Jayson, G. C. (2001) *Br. J. Cancer* **85,** 1094–1098
58. Selleck, S. B. (2001) *Semin. Cell Dev. Biol.* **12,** 127–134
59. Iozzo, R. V. (2005) *Nat. Rev. Mol. Cell. Biol.* **6,** 646–656
60. Häcker, U., Nybakken, K., and Perrimon, N. (2005) *Nat. Rev. Mol. Cell. Biol.* **6,** 530–541
61. Fernàndez-Busquets, X., and Burger, M. M. (1999) *Microsc. Res. Tech.* **44,** 204–218
62. Fernàndez-Busquets, X., Kuhns, W. J., Simpson, T. L., Ho, M., Gerosa, D., Grob, M., and Burger, M. M. (2002) *Dev. Comp. Immunol.* **26,** 313–323
63. Bershadsky, A. D., Balaban, N. Q., and Geiger, B. (2003) *Annu. Rev. Cell Dev. Biol.* **19,** 677–695
64. Tan, J. L., Tien, J., Pirone, D. M., Gray, D. S., Bhadriraju, K., and Chen, C. S. (2003) *Proc. Natl. Acad. Sci. U. S. A.* **100,** 1484–1489